Analysis of Quadratic Transfer Functions in Operability Studies for Heavy Lift Operations

Auteur : Wirautama, Galura
Promoteur(s) : Rigo, Philippe
Faculté : Faculté des Sciences appliquées
Diplôme : Master : ingénieur civil mécanicien, à finalité spécialisée en "Advanced Ship Design"
Année académique : 2024-2025
URI/URL : http://hdl.handle.net/2268.2/25048

Analysis of Quadratic Transfer Functions in Operability Studies for Heavy Lift Operations

submitted on 16 August, 2025

by

WIRAUTAMA, Galura

Supervisor:

Alufa Samson Olorunfemi
DEME Offshore

First Reviewer:

Guillaume Ducrozet
Professeur des universités
44470 Nantes
France

Second Reviewer:

Vincent Leroy
Maître de conférences
44470 Nantes
France

[This page is intentionally left blank]

Contents

List of Figures

List of Tables

List of Abbreviations

Abbreviation	Definition
BEM	Boundary Element Method
BV	Bureau Veritas
CoG	Center of Gravity
DOF	Degree of Freedom
DP	Dynamic Positioning
ECN	École Centrale de Nantes
FLNG	Floating Liquefied Natural Gas
FPSO	Floating Production Storage Offloading
FS	Free Surface
GM	Metacentric Height
HLV	Heavy-Lift Vessel
Hs	Significant Wave Height
JONSWAP	Joint Offshore North Sea Wave Project
LC	Loading Condition
LCG	Longitudinal Center of Gravity
LMP	Lifting Monopile
MPM	Most Probable Maximum
NREL	National Renewable Energy Laboratory
QTF	Quadratic Transfer Function
RAO	Response Amplitude Operator
TCG	Transverse Center of Gravity
TLP	Tension-Leg Platform
Tp	Peak Period
VCG	Vertical Center of Gravity
WMP	Without Monopile

Nomenclature

Symbol	Definition	Units
a	Wave amplitude, real	[m]
A	Wave amplitude, complex	$[m]$
B	Radiation damping	[kg/s]
d	Water depth	[m]
D	Wave spreading function	
F	Force	$[N]$
g	Gravitational constant	$[m/s^2]$
G	Center of gravity coordinates in global frame	[m]
k	Wave number	$[1/m]$
m_j	j-th order moment of spectrum	[]
M	Mass	[kg]
M_a	Added mass	[kg]
M_e	External Moment	$[N.m]$
n	Outward normal vector in body frame	[]
N	Outward normal vector in global frame	[]
p	Pressure	$[N/m^2]$
P_{oi}	Coordinates of point of interest	[m]
Q_{TF}	Quadratic Transfer Function	[N or Nm/m^2]
R	Linearized rotation matrix	[]
RAO_{Load}	Load response amplitude operator	[N or Nm/m]
RAO_{Motion}	Motion response amplitude operator	$[mor^o/m]$
s	Elementary surface discretization	[m]
S	Wave Spectrum	$[m^2/s]$
S_R	Response Spectrum	[]
S_B	Wetted Body Surface Mesh	[]
t	Time	$[s]$
v	Velocity	$[m/s^2]$
x	x axis displacement in body frame	$[m]$
X	x axis displacement in body frame	$[m]$
$[X]$	displacement vector in cartesian coordinates	$[m]$

$[\dot{X}]$	velocity vector in cartesian coordinates	$[\frac{m}{s}]$
$[\ddot{X}]$	velocity vector in cartesian coordinates	$[\frac{m}{s^2}]$
y	y axis displacement in body frame	$[m]$
Y	y axis displacement in global frame	$[m]$
z	z axis displacement in body frame	$[m]$
Z	z axis displacement in global frame	$[m]$
β	Wave direction	$[^o]$
γ	Peakedness parameter	[]
Γ	Elementary waterline discretization	[]
ϵ	Perturbation parameter	[]
ζ	Heave displacement of body	$[m]$
η	Free surface elevation	[m]
θ	Pitch displacement	$[^o]$
μ	Mean value	[]
ρ	Density	$[kg/m^3]$
σ	Standard Deviation	[]
ϕ	Roll displacement	$[^o]$
Φ	Fluid velocity potential, real	[]
ψ	Yaw displacement	$[^o]$
Ψ	Assisting function from 1^{st} order radiation potential	[]
ω	Angular frequency	$[rad/s]$
ω_n	Natural frequency	$[rad/s]$
∇	Gradient operator in cartesian coordinates	[]
φ	Phase	$[^o]$

[This page is intentionally left blank]

DECLARATION OF AUTHORSHIP

I, **GALURA WIRAUTAMA** declare that this thesis and the work presented in it are my own and have been generated by me as the result of my own original research.

Where I have consulted the published work of others, this is always clearly attributed.

Where I have quoted from the work of others, the source is always given. With the exception of such quotations, this thesis is entirely my own work.

I have acknowledged all main sources of help.

Where the thesis is based on work done by myself jointly with others, I have made clear exactly what was done by others and what I have contributed myself.

This thesis contains no material that has been submitted previously, in whole or in part, for the award of any other academic degree or diploma.

I cede copyright of the thesis in favour of DEME Offshore.

Date: 16 August 2025

Signature: Galura Wirautama

[This page is intentionally left blank]

ABSTRACT

Current industry standards for vessel motion analysis commonly considers only 1^{st} order diffraction analysis. This assumes that external excitation only occurs at the incident wave frequencies and thus natural modes outside of the wave frequency range would not be excited. However, in some cases, research have shown that 2^{nd} order effects could still induce resonances despite being outside of the wave frequency range. The lifting of a monopile by an offshore heavy-lift vessel (HLV) could be one such case where, due to an upwards shift of the vertical center of gravity (VCG) as the monopile is lifted, the natural frequency of roll falls below and outside of the incident wave frequency range.

This thesis presents a calculation and analysis of the effects of including quadratic transfer functions (QTFs) in a heavy-lift analysis. In the beginning of the thesis, a comparison of QTFs is performed between two different software NEMOH and Orcawave for the simple geometry of a floating cylinder. This is done to validate the calculation results of Orcawave with NEMOH, whose calculation results have been verified in some publications. Then, mesh studies are performed on the vessel lid, vessel hull, and free surface to study their effects and convergence.

The first part of the main work of the thesis covers radiation-diffraction analyses performed on a heavy-lift vessel using Orcawave to obtain, analyse, and compare the 1^{st} and 2^{nd} order transfer functions of two loading conditions. An attempt to compare 1^{st} and 2^{nd} order loads for a given sea state in presented, as well as a rough attempt to compute and compare the 1^{st} and 2^{nd} order significant roll motions in a given range of incoming wave periods.

The second part of the main work of the thesis uses Orcaflex to perform time-domain simulations of the heavy lift. This allows modelling of flexible and multi-bodies and solves the complete equation of motion including both 1^{st} and 2^{nd} order excitations naturally. Separate simulations omitting and including QTFs are performed. The resulting motion response is analysed in both time and frequency domain to obtain the most probable maximum (MPM) roll motions and identify excitation of the natural modes. Two operability studies omitting and including QTFs are then carried out to obtain limiting wave heights by comparing the MPM roll motions against allowable limits. The results are analysed and compared to observe the effect of QTFs on operability of the heavy-lift.

Keywords: QTFs, 2^{nd} order loading, free surface mesh, mean drift, quadratic load, potential load, full QTFs, significant response, most probable maximum, limiting Hs

1 INTRODUCTION

This thesis aims to understand the effect of considering 2^{nd} order wave loadings to investigate the motions of a heavy-lift vessel during a lifting operation. To do so, quadratic transfer functions are computed using commercial diffraction code and analysed. Then together with the 1^{st} order response amplitude operators, they will be applied in the motion analysis for a lifting operation with the use of a nonlinear time-domain simulation. Through the study, the effects of including 2^{nd} order loads and moments, represented by QTFs, will be evaluated, especially on its impact towards the operability of a heavy-lift vessel during a lifting operation.

1.1 Problem Description

Motion analyses of a floating vessel in the offshore industry commonly considers only linear (1^{st} order) wave-structure interaction theory. However, the limitations of linear 1^{st} order theory are known and in some cases provide unsatisfactory prediction of vessel loading and motions. This often occurs when the natural frequencies of the motion fall outside the range of wave frequencies. A well known example of this is when performing mooring analyses on floating platforms. Their horizontal motions (surge, sway, yaw), which are to be restrained by the mooring, have long natural periods which are not excited by 1^{st} order theory but might be excited by the drift forces of 2^{nd} order.

Another 2^{nd} order phenomenon that is being increasingly investigated is the roll motion on Floating Production Storage and Offloading (FPSO) and Floating Liquified Natural Gas vessels (FLNG) vessels. Designers try to improve vessel motions by lowering the metacentric height and therefore roll stiffness of the vessel. This succeeded in moving the roll natural period outside the range of encountered wave periods. Unexpectedly, the vessels still experience roll motions. As evidenced by model tests and more recently numerical calculations, these motions are shown to be due to resonance induced by 2^{nd} order excitations [1] [2].

Looking at load cases where 2^{nd} order excitation might be a problem raises the issue of offshore heavy-lift operations. When a load is lifted, the load acts on the crane tip and therefore might significantly raise the vertical center of gravity of the vessel. This reduces the vessel's metacentric height and lowers the natural frequency of the rotational motions. At a first glance, this could be favorable since it would move the natural frequency outside

of the wave frequency range. However, it moves into the domain of low frequency motions and therefore it would be interesting to see whether 2^{nd} order loading could excite the roll resonance and significantly impact roll motions.

1.2 Thesis Scope

The main objective of the thesis is to investigate the effect of including 2^{nd} order loads via QTFs on the motion response and operability of an HLV. Several questions in general are put forward to limit the scope of the thesis; outside of these questions is considered beyond the scope of the thesis.

1. What are QTFs and how does it affect vessel motions?
2. How do 1^{st} order and 2^{nd} order loadings and motion responses compare?
3. What are the effects of including QTFs on a heavy-lift vessel's roll motion?
4. How is operability affected when QTFs are included in computing the vessel's roll motion responses?

Since 2^{nd} order loading is quite a complex topic, several assumptions are made to simplify the problem. First of all, forward speed is neglected in this thesis. Wind and current forces are also neglected to capture only motion effects due to wave loading. Additionally, since the matter of interest is the motion response of an HLV during a lifting operation, it is decided to analyse only the difference frequency effects while the sum-frequency effects will be neglected. This is based on the reasoning that difference-frequencies are more likely to induce long period, large amplitude motions which would significantly affect vessel operability, whereas sum-frequencies would more likely induce structural vibrations. Considering only the difference-frequencies will also lighten computational challenge and resource. While out of the scope of this thesis, it must be noted that sum-frequencies might also induce natural modes of the heavy lifting operation, in particular affecting the lifting equipment, which could contribute to vessel motions.

1.3 Thesis Outline

This thesis is organized into 5 chapters and a conclusion, detailed in the following:

- **Chapter 1** describes the background, problem, and motivation of the thesis. Its scope is defined, along with major assumptions that are made. An outline of the thesis is presented to provide clarity of the thesis structure to the reader.
- **Chapter 2** provides a review on the 1^{st} order diffraction - radiation problem, available 2^{nd} order formulations and approximations, as well as on sea state models to gain familiarity with the topic of 2^{nd} order wave loading and QTFs.

- **Chapter 3** covers the features of several software available to the author. A simple geometry testcase from an open-source BEM code is simulated with another commercial boundary element method (BEM) code. This is performed to gain some familiarity with QTFs and to have a starting point benchmark, as well as to decide the software that will be used in the master thesis.
- **Chapter 4** constitutes the first part of the main work of the master thesis. The vessel, loading conditions, and environmental parameters are presented. A mesh study is then performed to analyse the effect of varying mesh on 1^{st} and especially 2^{nd} order results and to obtain a working mesh. Next, a diffraction analysis is performed using a BEM code. An attempt to compare 1^{st} and 2^{nd} order loads for a given sea state is performed. Afterwards, an attempt to compute and compare the 1^{st} and 2^{nd} order significant responses are performed. All of this are performed in the frequency domain, with several simplifying and linearizing assumptions.
- **Chapter 5** makes up the second part of the main work of the thesis. A heavy-lift operation is simulated using a time-domain solver to include the dynamics of multi-bodies (the vessel and the lifted load). Computed RAO and QTFs from the previous chapter are imported into the time-domain solver to incorporate 1^{st} and 2^{nd} order wave excitation. 1^{st} order responses, 2^{nd} order responses, and 1^{st} plus 2^{nd} order responses are extracted, analysed and compared. Next, an operability study is carried out, computing the most probable maximum motions and limiting significant wave heights, to observe and compare the effect of including 2^{nd} order loading on an offshore heavy lifting operation.

A final chapter discusses the conclusions and future works that are obtained from this thesis.

2 THEORETICAL OVERVIEW

This chapter attempts to cover the theory and main assumptions relating to the topic of 2^{nd} order wave effects and quadratic transfer functions. It can be regarded as a summary of the works of Pinkster [3], Molin [4], Faltinsen [5], course materials on wave-structure interaction from ECN [6] and TU Delft [7], manuals and guidelines [8] [9] [10] [11] [12], as well as publications [13] [14] [15] [16] [17] [18] [19] [20]. First, frames of reference and conventions are presented. Then, a concise summary of the potential flow theory and the diffraction - radiation problem is given. Next, differences between the 1^{st} and 2^{nd} order assumptions and the resulting boundary value problems are highlighted. Afterwards, an elaboration on several 2^{nd} order load formulations is explained, followed by how they are represented by QTFs. Time-domain is briefly touched upon and then methods to model a sea state is introduced.

2.1 Frame of Reference and Conventions

An illustration of the wave-structure interaction problem can be illustrated as in Figure 2.1. Two frames of references are given, following the right hand notation.

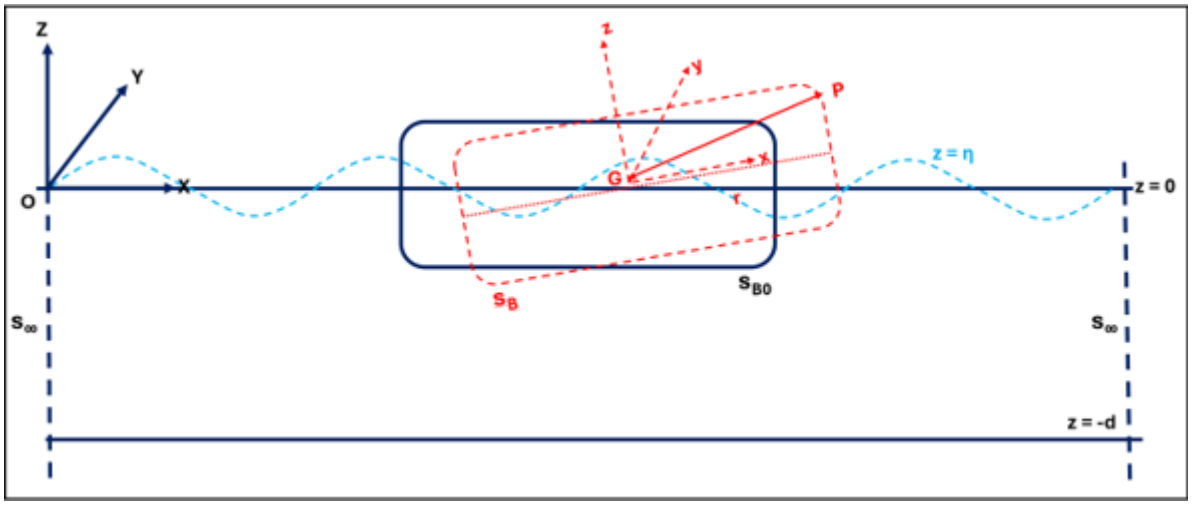

Figure 2.1: Illustration of Wave-Structure Interaction Problem with Two Frames of References OXYZ and Gxyz

1. A global earth-fixed frame of reference OXYZ, with axes denoted by capital letters. The origin is at the still water level. This frame does not move.

2. A body-fixed frame of reference Gxyz, with axes denoted by small letters. The origin is at the body's center of gravity. This reference moves with the body as it moves; in its mean position, the axes are parallel with the OXYZ frame of reference.

X, Y, Z are positive to bow, to port, and upwards, while rotations are positive counter-clockwise when facing towards the axis positive. Rigid body degree of freedoms are noted as surge (x), sway (y), heave (z), roll (ϕ), pitch (θ), and yaw (ψ).

2^{nd} order formulations are usually formulated using the Gxyz frame. When the body responds to 1^{st} order wave loads with small amplitude motions, the relation of a position of a point of interest on the surface of the body in the global and body frames are given by:

$$\overrightarrow{X} = \overrightarrow{G} + R \cdot \overrightarrow{x} \tag{2.1}$$

where $\overrightarrow{X}$ is the displacement vector of the point of interest in the global frame, $\overrightarrow{G}$ is the displacement vector of the center of gravity in the global frame, $\overrightarrow{x}$ is the position of the point of interest in the body frame, and R is the linearized rotation matrix. The same transformation process apply for other quantities of interest, for example velocity ($\overrightarrow{X}$) vector. R is given by:

$$R^{(1)} = \begin{bmatrix} 0 & -\psi^{(1)} & \theta^{(1)} \\ \psi^{(1)} & 0 & -\phi^{(1)} \\ -\theta^{(1)} & \phi^{(1)} & 0 \end{bmatrix} \tag{2.2}$$

The normal outward orientation of a surface element with respect to the moving body frame $\overrightarrow{n}$ is translated into the normal outward orientation of the fixed global frame by the following relation:

$$\overrightarrow{N} = R \cdot \overrightarrow{n} \tag{2.3}$$

2.2 Wave-Structure Interaction

2.2.1 Potential Flow Theory

This thesis considers the fluid around the structure to be incompressible and inviscid and that the flow around the structure is irrotational. This leads to potential flow theory, where the velocity field in the surrounding fluid can be derived from a scalar velocity potential Φ that satisfies Laplace's equation.

$$
\begin{aligned}
(\overrightarrow{v}) &= \nabla\Phi \\
\nabla(\nabla\Phi) &= 0 \\
\nabla^2\Phi &= 0 \qquad \text{within the fluid domain}
\end{aligned} \tag{2.4}
$$

Once the velocity field around the structure is known, the pressure field can be obtained using Bernoulli's equation for an unsteady flow:

$$p = p_0 - \rho g z - \rho\frac{\partial\Phi}{\partial t} - \rho\frac{1}{2}|\nabla\Phi|^2 \tag{2.5}$$

Integrating the pressure field on the surface of the structure interacting directly with the fluid (the submerged part) results in the external fluid force acting on the structure. Multiplying the fluid pressure and the lever arm w.r.t the center of mass and integrating on the submerged part we get the external fluid moment acting on the structure.

$$\overrightarrow{F} = \iint_{S_B} p\ \overrightarrow{n}\ ds \tag{2.6}$$

$$\overrightarrow{M} = \iint_{S_B} p\ \overrightarrow{GP_{oi}} \wedge\ \overrightarrow{n}\ ds \tag{2.7}$$

The potential flow assumption is less accurate for small or slender bodies in waves, since the forces induced by flow separation such as lift and drag is significant. These forces are not captured by potential flow theory as viscosity is neglected. Additionally, if wind and current are present to a point where their flow is separated by the presence of the vessel, viscous terms need to be considered.

For large bodies, forces generated by the diffraction and radiation of the body is significantly larger than viscous forces. As such, potential flow is considered valid and widely used for seakeeping analysis, including the analysis considered in this thesis.

2.2.2 Diffraction-Radiation Problem

The fluid flow due to the presence of waves around a floating structure is quite complex since it is a combination of the incoming wave, reflected wave, and waves generated by the motion response of the structure itself. To simplify the problem, linearity is assumed and so the total fluid potential Φ_T is broken down into the incident, diffracted, and radiated potential as described by equation 2.8.

$$\Phi_T = \Phi_I\ +\ \Phi_D\ +\ \Phi_R \quad \text{where} \quad \Phi_R = \sum_{j=1}^{6} \dot{x}_j \Phi_{R,j} \tag{2.8}$$

Φ_T is the total fluid potential, Φ_I is the undisturbed incident wave potential, Φ_R is the

potential due to the waves generated by the motion of the body in calm water for each DOF j (total 6 DOF for an unrestrained rigid body), and Φ_D is the remaining potential of the waves disturbed by the body or "diffracted" waves. Each of these apply a force onto the body:

$$\overrightarrow{F_T} = \overrightarrow{F_I} + \overrightarrow{F_D} + \overrightarrow{F_R} \tag{2.9}$$

F_T is the total force, F_I is the force due to the undisturbed incident pressure (also known as the Froude-Krylov force), F_D is the force due to wave diffraction, and F_R is the force due to the radiated waves. F_I and F_D can be obtained by integrating the pressure field of the undisturbed incident and diffracted waves. The radiation force is quite different in the sense that it is caused by waves generated by the motion of the body in calm water along each DOF and the resulting force can be composed into two components, namely the added mass and radiation damping. The forces are given by:

$$\overrightarrow{F_I} = \rho \iint_{S_{B,0}} \Phi_I \ \overrightarrow{n} \ ds \tag{2.10}$$

$$\overrightarrow{F_D} = \rho \iint_{S_{B,0}} \Phi_D \ \overrightarrow{n} \ ds \tag{2.11}$$

$$\overrightarrow{F_R} = \rho \iint_{S_{B,0}} \Phi_R \ \overrightarrow{n} \ ds \quad = -\sum_{j=1}^{6} M_{a_{ij}} \ddot{x}_j - \sum_{j=1}^{6} B_{ij} \dot{x}_j \tag{2.12}$$

Once the forces are known, body motion response transfer functions can be predicted by solving a linearized equation of motion given in Equation 2.13.

$$RAO_{Motion}(\omega) = \frac{X(\omega)}{A} = \frac{(\overrightarrow{F_I} + \overrightarrow{F_D})(\omega)}{-\omega^2(M + M_a(\omega)) - i\omega B(\omega) + K(\omega)} \tag{2.13}$$

Since analytical expression of Φ_I is already known, solving for Φ_D and the radiation coefficients are the main goal of the diffraction-radiation problem. It can be modelled as a set of boundary value problems considering the free surface, the seabed, and the floating body as boundary conditions. The laplacian describes the velocity potential within the fluid domain. This set of equations is complex to solve and so simplifications, by linearization and truncation of the exact solution is performed based on perturbation series as shown in Equation 2.14.

$$\begin{aligned}
\Phi &= \Phi^{(0)} + \epsilon\Phi^{(1)} + \epsilon^2\Phi^{(2)} + \epsilon^3\Phi^{(3)} + ... \\
\eta &= \eta^{(0)} + \epsilon\eta^{(1)} + \epsilon^2\eta^{(2)} + \epsilon^3\eta^{(3)} + ... \\
F &= F^{(0)} + \epsilon F^{(1)} + \epsilon^2 F^{(2)} + \epsilon^3 F^{(3)} + ... \\
X &= X^{(0)} + \epsilon X^{(1)} + \epsilon^2 X^{(2)} + \epsilon^3 X^{(3)} + ...
\end{aligned} \tag{2.14}$$

The perturbation term ϵ in this context corresponds to the wave steepness kA which is $<< O(1)$. The number of terms that will be kept depends on the order of problem that is desired to be solved; for example, linearized 1^{st} order problems will only keep terms of order (0) and (1).

The assumptions and simplifications made for 1^{st} and 2^{nd} order problems, which is the main topic of this thesis, will be elaborated in the following subsections.

1st Order Problem

In 1^{st} order theory, linearization is performed by considering only the static (0^{th} order) and 1^{st} order terms of the perturbation series (corresponding to the first two terms in Equation 2.14). The 2^{nd} order and higher order terms are ignored. This simplification is sufficiently accurate in many common problems of ocean engineering and is the current industry standard. However, some simplifying assumptions are made and when these assumptions do not hold anymore, 1^{st} order modelling will provide a noticeable error. The following assumptions are made for 1^{st} order theory:

1. A small amplitude regular wave is acting on the body.
2. The body is initially stationary.
3. The body motion response is small and at the same frequency as the incident wave.
4. There is a constant mean waterline of z = 0.
5. A linearized free surface and body boundary condition is assumed.
6. Bernoulli's quadratic pressure term is omitted.

The following Equations 2.15 - 2.19 describe the boundary conditions of the linearized 1^{st} order problem:

$$\nabla^2\Phi^{(1)} = 0 \qquad \text{everywhere in the fluid domain} \tag{2.15}$$

$$\frac{\partial^2\Phi^{(1)}}{\partial t^2} + g.\frac{\partial\Phi^{(1)}}{\partial z} = 0 \qquad \text{at z = 0} \tag{2.16}$$

$$\frac{\partial\Phi^{(1)}}{\partial z} = 0 \qquad \text{at z = -d} \tag{2.17}$$

$$\overrightarrow{\nabla}\Phi^{(1)}.\overrightarrow{n} = \dot{X}_B^{(1)}.\overrightarrow{n} \qquad \text{at body surface } S_b \tag{2.18}$$

$$\lim_{r\to\infty}\frac{\partial(\Phi^{(1)} - \Phi_I^{(1)})}{\partial r} \to 0 \qquad \text{at fluid domain boundary } S_\infty \tag{2.19}$$

The fluid potential due to the undisturbed incident regular wave, which is the solution of the above boundary value problem without the presence of a body (omitting Equation 2.18 and Equation 2.19), is known by solving the boundary value problem given in Equations

2.15 - 2.17. For a wave frequency of ω and amplitude A, the 1^{st} order incident potential Φ_I is given by:

$$\Phi_I^{(1)} = \Re\left\{-i\frac{Ag}{\omega}\frac{cosh(k(z+d))}{cosh(kd)}e^{i(kx-\omega t)}\right\} \tag{2.20}$$

2nd Order Problem

2^{nd} order theory now includes the first three terms from Equation 2.14, while higher order terms are still ignored. The main difference with 1^{st} order is that as a base case, the incident waves are bichromatic waves. The wave-wave interaction are now considered in the boundary conditions and excites additional loads on the body at frequencies other than their own. The following points summarize the difference that arises when considering 2^{nd} order theory:

1. Bichromatic wave acting on the body is taken as a base case.
2. The body is already responding to a harmonic 1^{st} order wave excitation.
3. There is an instantaneous waterline on the body which, when measured over time, may not have its mean at z = 0 (still waterline).
4. Excitation and response is imposed at difference and sum frequencies.

2^{nd} order loads increase quadratically with the increase of the wave height due to the perturbation factor ϵ^2. Additionally, due to the wave-wave interactions, several terms appear in the body and free surface boundary conditions. The boundary conditions for the 2^{nd} order theory is given in Equations 2.21 - 2.25:

$$\nabla^2\Phi^{(2)} = 0 \qquad \text{everywhere in the fluid domain} \tag{2.21}$$

$$\frac{\partial^2\Phi^{(2)}}{\partial t^2} + g.\frac{\partial\Phi^{(2)}}{\partial z} = Q_F \qquad \text{at z = 0} \tag{2.22}$$

$$\frac{\partial\Phi^{(2)}}{\partial z} = 0 \qquad \text{at z = -d} \tag{2.23}$$

$$\overrightarrow{\nabla}\Phi^{(2)}.\overrightarrow{n} - \dot{X}_B^{(2)}.\overrightarrow{n} = Q_B \qquad \text{at body surface } S_b \tag{2.24}$$

$$\lim_{r\to\infty}\frac{\partial(\Phi^{(2)} - \Phi_I^{(2)})}{\partial r} \to 0 \qquad \text{at fluid domain boundary } S_\infty \tag{2.25}$$

Q_F and Q_B in Equations 2.22 and 2.24 are free surface and body *forcing terms*, given by:

$$Q_F = -2\nabla\Phi^{(1)}.\nabla\frac{\partial\Phi^{(1)}}{\partial t} + \frac{\partial\Phi^{(1)}}{\partial t}\left(\frac{\partial^2\Phi^{(1)}}{\partial Z^2} + \frac{1}{g}.\frac{\partial^2}{\partial t^2}\left(\frac{\partial\Phi^{(1)}}{\partial Z}\right)\right) \tag{2.26}$$

$$Q_B = (\dot{X}^{(1)} - \nabla\Phi^{(1)}).\overrightarrow{N}^{(1)} - (X^{(1)}.\nabla).(\nabla\Phi^{(1)}.\overrightarrow{n}) \tag{2.27}$$

The free surface forcing term attempts to accommodate the interaction of a free and bound wave. Since the body is already moving in response to 1^{st} order wave excitation, the effect of the relative motion of the body and the fluid on the fluid potential is described by this body forcing term. These terms are absent in the 1^{st} order linear problem since the body is considered initially static and that there are no free - bound wave interactions present that alters the surface elevation of the regular waves.

The 2^{nd} order incident potential, also known analytically, for a wave with frequency of ω and amplitude A is given by:

$$\Phi_I^{(2)} = \Re\left\{-i\frac{3A^2\omega}{8}\frac{cosh(2k(z+d))}{sinh^4(kd)}e^{2i(kx-\omega t)}\right\} \tag{2.28}$$

Solving the above boundary value problems with the added presence of the body and surface forcing terms to obtain the 2^{nd} order diffraction and radiation potentials is extremely difficult. As such, approximations are commonly applied to estimate the loads arising from 2^{nd} order potential without solving for the diffracted and radiated potentials themselves. Some of the widely used approximations include the indirect method and Pinkster's approximation formulated by Bernard Molin and J.A Pinkster, respectively. These approximations will be expanded in a later section (section 2.3.3).

2.3 Computation of 2nd Order Loads

Computing 2^{nd} order wave loading is complex since unlike 1^{st} order loading and response, more terms are taken into account. In general, 2^{nd} order wave loading is composed of the quadratic and potential load components:

$$\overrightarrow{F}_T^{(2)} = \overrightarrow{F}_Q^{(2)} + \overrightarrow{F}_P^{(2)} \tag{2.29}$$

The quadratic load component represents the loads arising due to the pre-existing body motion response towards 1^{st} order waves. This constitutes the main difference with 1^{st} order loading which assumed the body as initially still. Quadratic loads are composed only of terms which can be derived from 1^{st} order solutions (1^{st} order potential and body motions). Motion RAOs are also required to describe the pre-existing body motion in response to incoming regular waves. As such, the full 1^{st} order problem needs to be resolved before 2^{nd} order analysis can be performed.

A few formulas have been developed to compute quadratic loads. However, approximations are commonly used to estimate the potential loads due to the complexity of the boundary value problem including the body and free surface forcing terms. The far-field and near-field formulations to compute the mean drift and quadratic load components are explained in the following sections. To compute the potential load component, the indirect method and Pinkster's approximation are also presented.

2.3.1 Maruo-Newman Formulation (Far-Field Method)

The *far-field method* is one of the earliest formulation available to compute 2^{nd} order quadratic loads. It was initially developed by Maruo for a 2D body, and later expanded by Newman for a 3D arbitrary body. Similar in principle to the Haskind load RAO formulation, this method computes quadratic loads by considering conservation of momentum of the fluid at the boundary of the domain which acts as a surrounding control surface (S_∞). The formulation can be seen in Equation 2.30:

$$\overrightarrow{F_Q}^{(2)} = \frac{1}{T}\int_0^T \Bigg\{ -\int_{\Gamma_\infty} \frac{1}{2}\rho g \eta^{(1)^2}\ \overrightarrow{n}\ d\Gamma + \iint_{S_\infty} \rho \left[\frac{1}{2}|\nabla\Phi^{(1)}|^2\ \overrightarrow{n} - \nabla\Phi^{(1)}\frac{\partial\Phi^{(1)}}{\partial n}\right] dS \Bigg\} dt \tag{2.30}$$

A major shortcoming of this formulation is that it can only compute the drift forces of the horizontal degrees of freedom which are surge, sway, and yaw. Additionally, it can only compute the loads for the case of a single floating body. This method is a widely available feature in several software, such as Ansys AQWA and Orcawave, but its use is mainly applicable for mooring analysis due to the significance of the horizontal motions.

A more recent adaptation of the far-field method which evaluates momentum conservation at an intermediary boundary surface has been formulated by X.B.Chen. It is known as the middle-field method and has the advantage of being able to compute all 6 DOFs. However, it requires an additional intermediary surface mesh which might add to computational expense.

2.3.2 Pinkster's Formulation (Near-Field Method)

The *near-field method* was derived by J.A. Pinkster in 1980. This method computes the quadratic loads by directly integrating the pressure acting on the hull including quadratic terms. It is given by the following formula:

$$\begin{aligned}\overrightarrow{F_Q}^{(2)} =& \frac{1}{2}\rho g \int_{\Gamma_0} \left(\eta^{(1)} - \zeta^{(1)}\right)^2 \overrightarrow{n}\ d\Gamma \\ &- \rho \iint_{S_B} \frac{1}{2}|\nabla\Phi^{(1)}|^2 \cdot \overrightarrow{n}\ ds \\ &- \rho \iint_{S_B} \overrightarrow{X}^{(1)} \cdot \nabla\frac{\partial\Phi^{(1)}}{\partial t} \cdot \overrightarrow{n}\ ds \\ &- \rho \overrightarrow{R} \wedge \iint_{S_B} \frac{\partial\Phi^{(1)}}{\partial t}\overrightarrow{n}\ ds\end{aligned} \tag{2.31}$$

The formulation can be broken down into the 4 distinct terms. An explanation of the physical meaning of each term, numbered from top to bottom, is given below:

1. Relative waterline contribution term –> 1^{st} order hydrodynamic forces up to the instantaneous waterline;
2. Pressure drop due to 1^{st} order velocity potential (from Bernoulli's equation);
3. Pressure due to coupling of first order pressure and motion;
4. Inertia force due to first order rotation;

Terms 3 and 4 arise from considering that the body is now moving in response to the waves. At higher frequencies they disappear since the body does not have time to respond to each individual wave and thus it stays still. This can be seen from Figure 2.2 which show the behaviour of each term at varying frequencies for a barge.

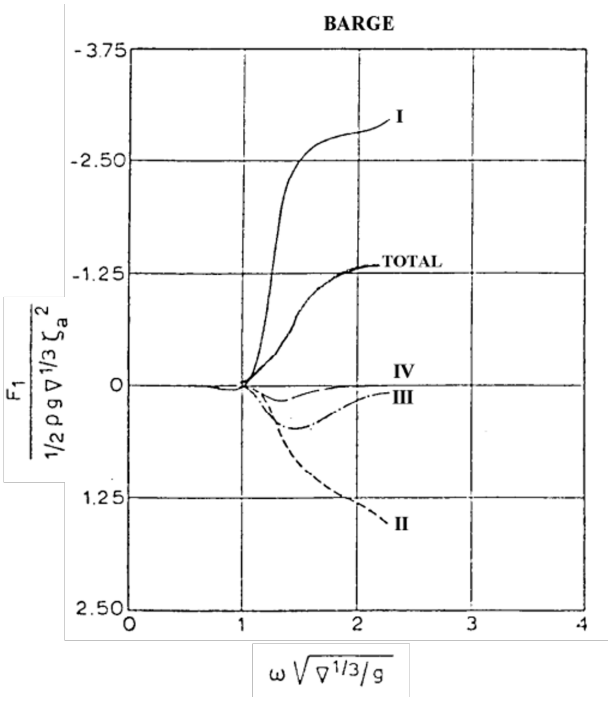

Figure 2.2: Behaviour of Terms from Pinkster's Formula [3]

There is an extra term which arises due to the hydrostatic components of the quadratic first order motions. In this thesis it is written as $F^{(2)}_{hsq1}$. This additional term is applied in some software but omitted in others.

The near-field formulation allows to solve for all 6 DOFs as well as for cases of multiple floating bodies. Due to its versatility, it is widely used in numerical code and commercial software as the basis to compute QTFs (such as in WAMIT, NEMOH, Orcawave). However, the mesh of the floating body must be sufficiently dense to avoid computational errors, increasing computational resource requirements.

2.3.3 Indirect Method to Compute 2nd Order Potential Load

Computing the 2^{nd} order potential load component given in Equation 2.29 is difficult due to the presence of the forcing terms in the boundary conditions. The free-surface forcing given by Equation 2.26 in particular makes it computationally expensive since a mesh of the free surface is required and is quite slow to converge.

Due to the complexity of the problem, solving the 2^{nd} order radiation problem is not performed. As such, it is usually accepted that the 2^{nd} order potential and load is represented by the incident and diffracted components:

$$\Phi^{(2)} = \Phi_I^{(2)} + \Phi_D^{(2)} \tag{2.32}$$

$$F_P^{(2)} = F_I^{(2)} + F_D^{(2)} \tag{2.33}$$

Two available methods to compute the potential component in the near field formulation are briefly explained in the following section.

Incident Potential Load

Similar to 1^{st} order, the load due to the 2^{nd} order undisturbed incident potential is given by a 2^{nd} order Froude-Krylov force:

$$\overrightarrow{F_I}^{(2)} = \iint_{S_B} \frac{\partial \Phi_I^{(2)}}{\partial t} \overrightarrow{n}\, ds \tag{2.34}$$

Diffracted Potential Load

The indirect method, formulated by Bernard Molin, is given in Equation 2.35. It computes the loads due to the 2^{nd} order diffracted potential using an assisting function Ψ obtained from first order radiation solutions at frequencies of $\Delta\omega$ coupled with the forcing terms.

$$\begin{aligned} \overrightarrow{F_D}^{(2)} &= \iint_{S_B} \Phi_D^{(2)} \overrightarrow{n_j}\, ds \\ &= \iint_{S_B} [\frac{\partial \Phi_I^{(2)}}{\partial n} - Q_B].\Psi_j - \frac{1}{g} \iint_{S_F} Q_F.\Psi_j\, ds \end{aligned} \tag{2.35}$$

The formula contains two integral terms; one over the body and one over the free surface. The integral over the body is possible since a body mesh is present. However, the second term requires a mesh of the free surface around the body to solve and is usually slow to converge. This represents the uniqueness and added computational expense of a full 2^{nd} order analysis.

2.3.4 Pinkster's Approximation

Pinkster's approximation assumes that the loads from 2^{nd} order potential are mainly due to the undisturbed incoming waves. It applies a scaling factor to first order wave loads based on the incoming wave frequency, wave number, and amplitude. The approximation is given in Equation 2.36:

$$\overrightarrow{F}^{(2)}_{jk}(t) = f_{jk} \cdot \overrightarrow{F}^{(1)}(k_j - k_k) \tag{2.36}$$

where

$$f_{jk} = \frac{a_j a_k A_{jk}(\omega_j - \omega_k)}{g}$$

$$A_{jk} = \frac{1}{2} g^2 \frac{B_{jk} + C_{jk}}{(\omega_j - \omega_k) - (k_j - k_k).g.tanh(k_j - k_k)d}$$

$$B_{jk} = \frac{k_j^2}{\omega_j cosh^2 k_j d} - \frac{k_k^2}{\omega_k cosh^2 k_k d}$$

$$C_{jk} = \frac{2k_j k_k(\omega_j - \omega_k)(1 + tanh(k_j d)\ tanh(k_k d))}{(\omega_j \omega_k)}$$

Pinkster's approximation is convenient since only the known wave characteristics A, k, and ω are required to estimate the 2^{nd} order potential loads. This saves a lot of computational expense because a mesh of the free-surface is not required. However, it should be noted that several studies have shown the shortcoming of this method, especially in shallower waters. It also fails to give a good approximation when the DOF of interest have higher natural frequencies ($\geq$ 0.1 rad/s). Therefore, this method could be considered for a first stage design where an approximation is sufficient and time is significantly more important than accuracy.

2.4 Quadratic Transfer Functions (QTFs)

Quadratic transfer functions are similar to wave load RAOs in the sense that they take wave frequency and amplitude as input and outputs the resulting 2^{nd} order loads. However, QTFs do this for a pair of waves with each of their own frequencies and directions $(\omega_1, \omega_2, \beta_1, \beta_2)$. This causes the loads to fluctuate quadratically, since two wave amplitudes are input. It also allows to apply 2^{nd} order wave loads in irregular waves.

QTFs outputs an excitation load for each DOF in the sum-frequency $(\omega_1 + \omega_2)$ or difference-frequency $(\omega_1 - \omega_2)$. When the two wave frequencies are the same, the difference frequency excitation become a zero-frequency, constant force known as the mean drift force. The sum frequency excitation for the two waves with the same frequency acts at the double frequency.

Equation 2.37 show the 2^{nd} order force exerted by a bichromatic wave made up of two regular waves with amplitudes A_1, A_2 and frequencies ω_1, ω_2:

$$\begin{aligned}\overrightarrow{F}^{(2)}(\omega_1,\omega_2,t) =& A_1^2\overrightarrow{Q_{TF_D}}(\omega_1) + A_2^2\overrightarrow{Q_{TF_D}}(\omega_2) \\ &+ \{A_1^2\overrightarrow{Q_{TF_+}}(\omega_1,\omega_1)e^{-2i\omega_1 t} \\ &+ \{A_2^2\overrightarrow{Q_{TF_+}}(\omega_2,\omega_2)e^{-2i\omega_2 t} \\ &+ 2A_1A_2\overrightarrow{Q_{TF_-}}(\omega_1,\omega_2)e^{-i(\omega_1-\omega_2)t} \\ &+ 2A_1A_2\overrightarrow{Q_{TF_+}}(\omega_1,\omega_2)e^{-i(\omega_1+\omega_2)t} \end{aligned} \tag{2.37}$$

QTFs for the mean drift forces, which do not depend on time, are represented by $\overrightarrow{Q_{TF_D}}$. $\overrightarrow{Q_{TF_{+-}}}$ represent the QTFs of the time-varying quadratic and potential load components. The subscripts + and - indicate sum and difference frequencies.

Mean Drift Loads

A bichromatic wave with the same frequency ($\omega_1 = \omega_2$) can result in a difference-frequency of $\omega_1 - \omega_2 = 0$ meaning that there is a time-independent force. These are known as the mean drift loads and they cause the mean offset of a body from its mean position. The mean drift loads are responsible for large loads in the horizontal degrees of freedoms, and as such they are often included in mooring design and analysis.

Difference-Frequency Loads

Difference-frequency loads take place at $\omega_1 - \omega_2$ frequency. The difference frequency loads are of great interest since it explains the excitation of low frequency natural periods of floating vessels. Especially for structures designed with long natural periods situated outside of the wave frequency range, a bichromatic wave which has a $\Delta\omega$ near to the natural frequency could excite the body's natural mode. It is particularly important to take into account the difference frequency loads in mooring design, in large vessels with long pitch and roll periods, and for dynamic positioning analysis of vessels.

Sum-Frequency Loads

Sum frequency loads take place at $\omega_1 + \omega_2$ frequency. They are commonly neglected in motion analyses, but could be of interest for structural engineers since the high frequency loads contribute to structural vibrations. Particular interest in sum-frequency effects concerns the excitation of low natural periods such as the effect of springing and ringing on tension-leg platforms (TLPs).

2.5 Time - Domain Simulation

It is not so straightforward to obtain a frequency domain transfer function for vessel motions (identical to motion RAOs) when considering 2^{nd} order wave loads. This is due to the presence of zero, difference, sum, and double frequency effects for each wave frequency combination present in the sea state. Therefore, to obtain vessel motions, a time-domain simulation is commonly performed where the sum of external forces arising from 1^{st} and 2^{nd} order wave loads can be resolved at each time-step to obtain vessel motions.

The equation of motion for a floating structure, considering both 1^{st} and 2^{nd} order forces is given in Equation 2.38:

$$([M] + [M_A])[\ddot{X}](t) + [B][\dot{X}](t) + [K_H][X](t) = [F_e^{(1)}](t) + [F_e^{(2)}](t) \tag{2.38}$$

Since time-domain simulations solve balance of forces at each time-step, the instantaneous horizontal and translation displacement of the vessel is calculated and used as the input at the next timestep. This causes some components of the quadratic load to be naturally captured in a time-domain simulation, since the instantaneous waterline elevation and body motions are computed and considered at each time step. As such, care must be taken so that the quadratic loads are not doubly computed when running a time-domain simulation with an imported QTF matrix. Some software have the feature to filter out common 2^{nd} order loads to avoid double counting and resulting in overestimation of motion responses.

2.5.1 Most Probable Maximum (MPM) Motions

The most probable maximum (MPM) motion is often used to compare extreme values from a time-domain simulation result. Using the mean and standard deviation, MPMs provides a response that is once exceeded over a certain number of events. Under the assumption that the roll motion follows a normal distribution and that the maxima follow a Rayleigh distribution, the MPM is given by Equation 2.39.

$$MPM = \mu + \sigma \sqrt{2\, ln\, n} \tag{2.39}$$

where the squared-root term corresponds to the MPM factor. n is the number of waves for a specified time duration which is usually determined by approximating 1000 wave events or by dividing the specified time period with the zero-crossing periods.

2.6 Sea State Models

Waves in the sea are random and change from time to time. Since linear wave theory is used, the random waves can be thought of as the sum of a number of regular wave

components. The free surface elevation in a random sea state is given in Equation 2.40:

$$\eta(t) = \Re\left\{\sum_{i=1}^{n} A_j \cdot e^{i(-\omega_j t+\varphi_j)}\right\} \tag{2.40}$$

A useful way to present sea states are through a wave spectrum, which can be obtained by applying fourier transform to a time-history measurement of the free surface. The wave spectrum is a power spectral density function of the free surface elevation of the random sea, describing the energy contained at each discrete wave frequency in the sea contributing to the overall shape of the sea surface.

$$S(\omega) = \frac{\frac{1}{2}a(\omega)^2}{\Delta\omega} \tag{2.41}$$

From this spectrum, some useful quantities can be extracted, such as the significant wave height (Equation 2.42) and the spectral moments (Equation 2.43)

$$H_s = 4\sqrt{m_0} \tag{2.42}$$

$$m_j = \int_0^\infty \omega^j \; S(\omega) \; d\omega \tag{2.43}$$

Once the spectral moments are known, the mean period (time between two crests / troughs) and zero up-crossing periods (time when the sea elevation crosses the zero reference point in the upwards direction) can be obtained.

$$\begin{aligned} T_z &= 2\pi\sqrt{\frac{m_0}{m_2}} \\ T_m &= 2\pi\sqrt{\frac{m_2}{m_4}} \end{aligned} \tag{2.44}$$

Some empirical formulas have been developed to generate a generalized wave spectrum. Among the most commonly used are the Pierson-Moskowitz and JONSWAP spectra, which will be detailed in the following subsections.

2.6.1 Pierson-Moskowitz Spectrum

The Pierson Moskowitz spectrum, also known as the ITTC or ISSC spectrum, gives a spectral shape for a fully developed sea state based on observations in the North Atlantic Ocean. The spectrum assumes that the fetch and time the wind has blown has been infinitely long. It is given by Equation 2.45:

$$S(\omega) = \frac{5}{16} H_s^2 \omega_p^4 \omega^{-5} \exp\left\{\frac{-5}{4}\left\{\frac{\omega}{\omega_p}\right\}^{-4}\right\} \tag{2.45}$$

2.6.2 JONSWAP Spectrum

The JONSWAP (Joint North Sea Wave Project) spectrum is one of the most well known and widely used spectrum in the offshore industry. This spectrum is suitable for areas of enclosed seas such as the North Sea. It is given by Equation 2.46:

$$S(\omega) = \frac{5}{16} H_s^2 \omega_p^4 \omega^{-5} \exp\left\{\frac{-5}{4}\left\{\frac{\omega}{\omega_p}\right\}^{-4}\right\} \gamma^{\exp\left\{-0.5\left\{\frac{\omega-\omega_p}{\sigma\omega_p}\right\}^2\right\}} \tag{2.46}$$

Based on the Pierson-Moskowitz spectrum, the JONSWAP spectrum models developing sea states by adding a peaked shape parameter γ. Within the peakedness parameter there is a spectral width parameter σ which is equal to 0.07 when $\omega \leq \omega_p$ and 0.09 when $\omega \geq \omega_p$.

The parameter allows to control the peakedness and thus concentration of the spectrum; a higher gamma would give a higher, more concentrated peak, typical of less developed seas. A lower gamma would give a less peaked, wider spectrum, indicating a more random sea surface elevation typical of developed sea states. A typical γ value is 3.3; for $\gamma = 1$, the JONSWAP spectrum becomes the Pierson-Moskowitz spectrum.

2.6.3 Directional Sea State

The sea spectrum given previously describes waves going in a single direction or known as a unidirectional spectrum. In reality, waves in a sea state could be going in different directions. To model the randomness, a simplification is usually made by assuming that the sea state is a sum of unidirectional spectra, each with different directions. This is given in Equation 2.47:

$$S(\omega, \beta) = S(\omega) D(\beta) \tag{2.47}$$

where D is the directional spreading function. A common spreading function for wind seas is given by Equation 2.48.

$$D(\beta) = \frac{\Gamma_w(1 + n/2)}{\sqrt{\pi \Gamma_w(1/2 + n/2)}} \cos^n(\beta - \beta_m) \quad \text{for} \quad -\frac{\pi}{2} \leq \beta - \beta_m \leq \frac{\pi}{2} \tag{2.48}$$

where Γ in this case is the Gamma function, β_m is the mean wave direction, and n is the wave spreading exponent.

3 FAMILIARIZATION WITH QTF SOFTWARE

A brief attempt to review and compare the computational capability of QTFs between some software will be discussed in this chapter. First of all, a review of the available software is carried out. Afterwards, a comparison is done by running a simple test case on the available software. The 1^{st} order motion RAOs are compared to capture any discrepancies, before running their 2^{nd} order modules. A comparison of the QTF matrices and off-diagonal is then carried out. Based on the comparisons, as well as the capability and convenience, a software will be chosen to carry out the further work of the thesis.

3.1 Available Software

Several numerical codes have been developed to calculate 2^{nd} order loads. Among the most well known commercial software capable of computing QTFs include WAMIT, HydroStar, SESAM, Orcawave, NEMOH, Ansys AQWA, DIFFRAC, among others. NEMOH stands out as being the only open source software which offers this feature [9].

In general, the listed software software are capable of computing the quadratic components using one or more of the formulas elaborated in Section 2.3. The differences commonly appear in the options and approximations offered; for example, the use of Pinkster's approximation or the option to include/omit the hydrostatic component of the quadratic 1^{st} order motion. Within the thesis, numerical codes accessible to the author which are NEMOH, Orcawave, and Ansys AQWA are discussed in the following subsections.

3.1.1 NEMOH

NEMOH is an open-source (BEM) code developed at ECN. It is able to compute hydrodynamic coefficients (added mass and potential damping), motion RAOs, and the full sum and difference frequency QTFs. As of August 2025, NEMOH is the only open-source BEM code that offers 2^{nd} order load computation capabilities through the release of NEMOH v3.0 which contains the NEMOH2 module in 2022.

NEMOH uses the near-field formulation to compute QTFs. It uses the computed 1^{st}

order motion RAOs to compute quadratic components of the 2^{nd} order loading. The potential component is computed using the indirect method as described in Equation 2.35. NEMOH has the option to compute only the quadratic components (DUOK), quadratic components + body forcing terms of the potential component (DUOK + HASBO), or the full QTFs (quadratic components + potential components considering both the body forcing and free surfacing forcing terms). It is also capable of including bi-directionality of waves and has the option to include or omit the hydrostatic terms of the quadratic first order motion when computing QTFs.

NEMOH estimates the inertia matrix required for computing the motion RAOs. It assumes that provided mesh is in equilibrium, computes the volume of the mesh to calculate the mass, and uses shell hypothesis as mentioned in NEMOH's online forum (issue #32) to estimate the inertia matrix. This is a very strong assumption which may not be suitable for some cases, for example ships which have a non-uniform distribution of loads along its length.

3.1.2 OrcaWave

Orcawave is a commercial diffraction software developed by Orcina Inc, which also developed the FEM-based mooring dynamics software Orcaflex. Orcawave is able to compute hydrodynamic coefficients, 1^{st} order load and motion RAOs, and full QTFs to compute loads due to the 2^{nd} order potential. By default, Orcawave includes the hydrostatic terms of the quadratic first order motion when computing QTFs.

Orcawave has the capability to import a body mesh from several formats including WAMIT's .gdf, NEMOH's .dat, Gmsh's .geo, and wavefront .obj files. The origin point of the imported geometry can be shifted or rotated with respect to the global origin of Orcawave by defining the "Mesh position" and "Mesh orientation". If neither shift nor rotation is applied, then the body origin coincides with the global origin.

Orcawave is also able to import an external FS mesh or generate its own. Without specifying an FS mesh, the full QTFs are computed without considering the free surface forcing terms, identical to NEMOH's DUOK + HASBO option.

The inertia matrix of the floating body is user-defined in Orcawave. It will be used to solve the equation of motion when computing motion RAOs, which in turn are inputs for the calculation of QTFs. Additional damping can be considered via an external damping matrix or by specifying a target percent of critical damping.

It must be kept in mind that Orcawave outputs its results at the origin of the body coordinates. Additionally, Orcawave's phasing is defined as a lead at the global origin, similar to WAMIT's, while NEMOH's is opposite to that. This indicates that the phase/imaginary part between NEMOH and Orcawave will be a mirror of each other.

3.1.3 Ansys AQWA

Ansys AQWA is a commercial software developed by Ansys Inc. It is among the most widely used diffraction software in the offshore industry. AQWA provides the option to compute quadratic components of QTFs using far-field or near-field formulation. In using the far-field formulation, only DOFs surge, sway, and yaw are solved and it works only for a single body. The near-field formulation option offers an alternative capable of solving all 6 DOFs and for multi-body cases. It also has the option to compute full QTFs. However, it only offers Pinkster's approximation to compute the potential component, represents a shortcoming of AQWA. Due to this limitation it is decided not to continue using Ansys AQWA, although investigating the tradeoff between accuracy and computational resource between the full QTF and the approximation would be quite interesting future work.

3.2 Software Comparison for a Simple Geometry

To compare the different software, as well as to get familiar with QTFs, the simple case of a floating cylinder, provided as testcase #8b_QTF_Cylinder in NEMOH's repository downloadable from GitLab [21], is simulated and analysed. The testcase represents a simple geometry which can be easily modelled in different software, and more importantly because there are reference results on the full QTF matrix as provided in [9]. The mesh of the floating cylinder and its details can be seen in Figure 3.1 and Table 3.1.

Table 3.1: Data from NEMOH testcase #8b_QTF_cylinder

Parameter	Value
Radius	6 m
Draft	14 m
Displacement	1625.87 ton
CoG (x, y, z)	[0, 0, 0]
CoB (x, y, z)	[0, 0, -7]

CoG and CoB are referenced to the mesh origin (0, 0, 0) which is at the center of the cylinder at the waterline. In this case, the CoG and the mesh origin coincide. The model was run in deep water (infinite water depth), for 100 wave frequencies starting from 0.01 - 1 Hz (0.0628 - 6.28 rad/s) and incidence of 0^o. Since the model is symmetric with respect to both the x and y axis, the pitch response from 0^o wave incidence would be the same as the roll response if given a 90^o wave incidence. To compare the different software, the testcase is run using NEMOH and Orcawave. Since NEMOH's results have already been published and validated by comparison with Hydrostar [9], NEMOH's results will serve as the benchmark.

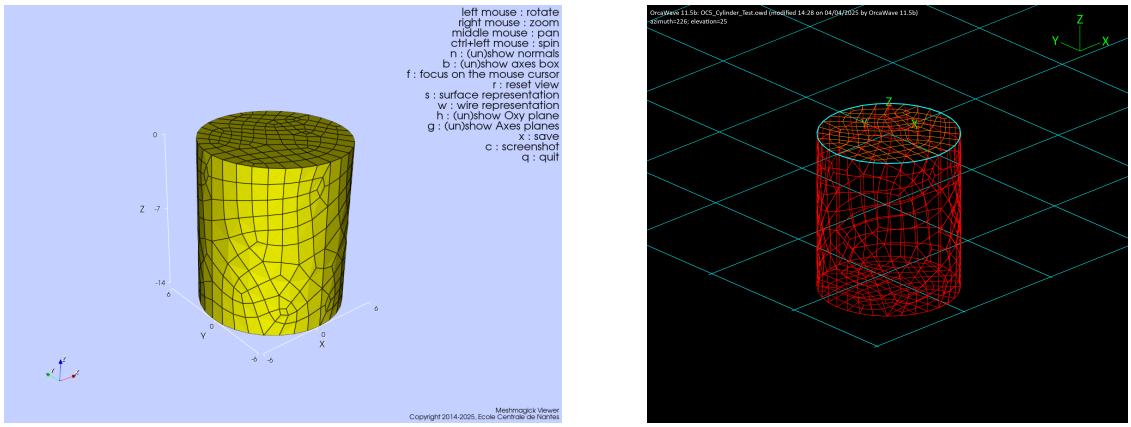

(a) NEMOH - Meshmagick [22] **(b)** Orcawave

Figure 3.1: Mesh of Testcase #8b_QTF_Cylinder

NEMOH

To run the testcase, NEMOH's executables are placed in the project folder together with the mesh.dat file, the Nemoh.cal file, the mesh.cal file, and the input_solver.txt file. The last three files contain the input solver settings for NEMOH's executables. The original setting as provided in the testcase is used with nothing changed. Once all the required files are present in the same folder, the executable files are run in a certain sequence, since some outputs are used as the input of other executables. The whole process to setup and run NEMOH in sequence is explained in [9].

The results of the hydrodynamic coefficients are output as .dat and .tec format, while the RAO and QTF are output as text in a .dat file. A python code was developed in order to plot the RAO and QTF results shown in this thesis.

Orcawave

Thanks to Orcawave's capability in importing geometries from different formats, the same NEMOH .dat file can be imported into Orcawave. No translation or rotation is applied and the global origin coincides with the body origin. The inertia matrix generated after running the same testcase in NEMOH is input into Orcawave. No additional damping is added.

No free surface mesh was specified in Orcawave. This omits the free surface forcing terms, making it identical to NEMOH's DUOK + HASBO option. Orcawave's QTF outputs are separated into the quadratic and potential components, given in phase and amplitude. To obtain the equivalent full QTF, they are decomposed into their real and imaginary parts, added together, and then transformed back into the full QTF phase and amplitudes. A python code has been developed to do this task.

The near-field formulation was used to compute the QTFs in Orcawave. The results will be shown in the following sections.

3.2.1 Comparison of Motion RAOs (1^{st} Order)

To start the comparisons, the 1^{st} motion RAOs are compared. Since the added mass, potential damping, excitation force, and inertia matrix are required to obtain the RAOs, matching RAOs would strongly suggest matching of individual hydrodynamic coefficients between the two software. Figure 3.2 shows the comparison of both the amplitude and phase RAO of the cylinder.

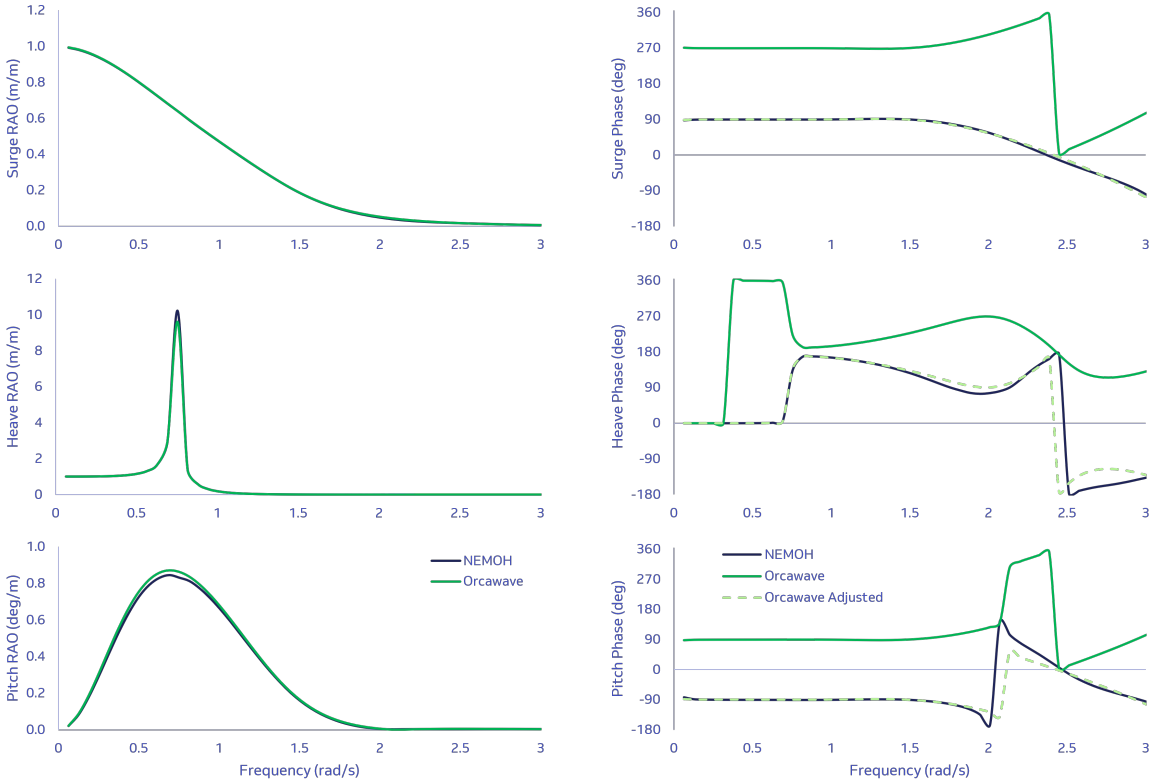

(a) Motion RAOs, Amplitudes **(b)** Motion RAOs, Phase

Figure 3.2: Comparison of Motion RAOs between NEMOH and Orcawave

Motion RAO amplitudes between NEMOH and Orcawave are observed to be almost identical, with only slight discrepancies observed around the resonance peak. On the other hand, discrepancies can clearly be seen in the phase RAO graphs. This can be explained by the fact that Orcawave uses a $0^o - 360^o$ phase wrapping, while NEMOH uses $(-180^o) - 180^o$. Additionally, as mentioned previously in Section 3.1.2, Orcawave and NEMOH use opposite conventions for the phase definition. Taking into account the different wrapping and opposite phases, the dashed line in the phase RAO graph presents the adjusted Orcawave phase RAOs. It can then be seen that they match well.

3.2.2 Comparison of QTFs (2^{nd} Order)

There are a few ways to compare QTFs. One of them is by comparing the QTF matrix visually, and another one would be to select and plot a certain off-diagonal. However,

since there would be too many off-diagonals to plot for a thorough comparison, in this case a visual comparison would be used where the QTF matrices will be plotted and compared. Afterwards, a comparison for constant difference frequency of $\Delta\omega = 0.189$ rad/s, corresponding to the pitch natural frequency of the cylinder, is performed. The pitch DOF is taken as a comparison here since this thesis is interested in the rotational motion (particularly roll). Additionally, as already mentioned in Section 1.2, only difference frequency QTFs are presented.

A python code was developed, inspired by the matlab wrapper provided in [9] to plot the QTF outputs from NEMOH. A similar code was independently developed to plot the QTF outputs from Orcawave. The Orcawave results are also normalized by density and gravity similar to NEMOH's.

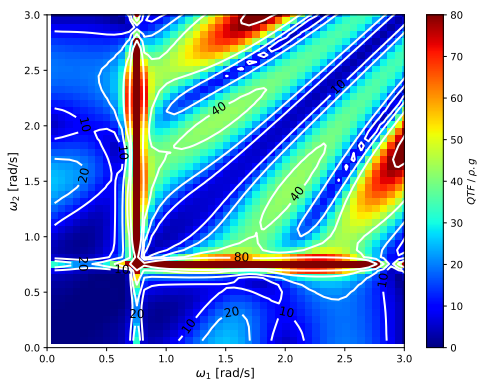

(a) NEMOH Pitch QTF

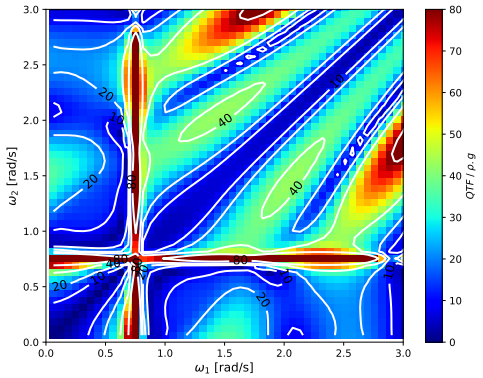

(b) NEMOH Pitch QTF with $F^{(2)}_{hsq1}$

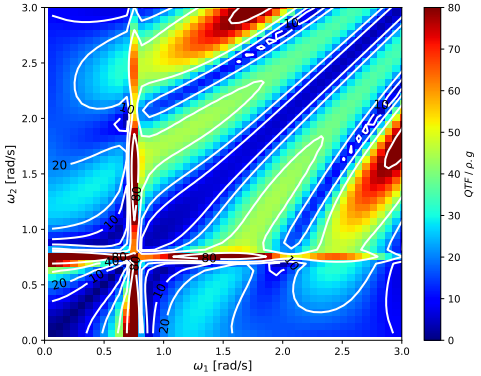

(c) Orcawave Pitch QTF

Figure 3.3: Comparison of Pitch QTFs between NEMOH and Orcawave

Figure 3.3 show a comparison of the QTF values between NEMOH and Orcawave. Some differences can be observed between Figure 3.3a and 3.3c, especially at the lower frequency range of 0.5 - 1.0 rad/s. A reason is because Orcawave, by default, includes the hydrostatic component of the 1^{st} order motions in its calculations, while the user is free to include it or not in NEMOH (known as $F^{(2)}_{hsq1}$). Once this component is toggled on in NEMOH as

seen in Figure 3.3b, the lower frequency range of 0.5 - 1.0 rad/s can be seen to be much more similar to the Orcawave QTF matrix.

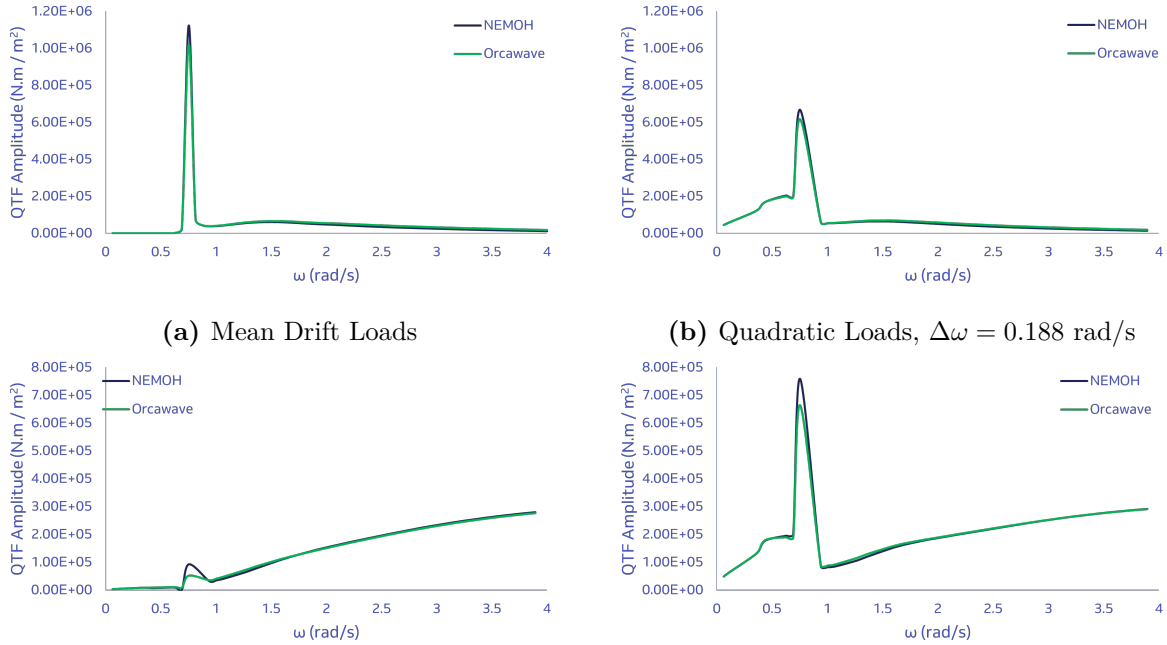

(a) Mean Drift Loads

(b) Quadratic Loads, $\Delta\omega = 0.188$ rad/s

(c) Potential Load, $\Delta\omega = 0.188$ rad/s

(d) Full QTF, $\Delta\omega = 0.188$ rad/s

Figure 3.4: Comparison of NEMOH and Orcawave QTF components

Figures 3.4 show the mean drift and diagonals at a constant $\Delta\omega$ of 0.188 rad/s which correspond to the pitch natural frequency of the cylinder. It can be observed that the mean drift, quadratic loads, potential loads (subject to body forcing terms only), as well as the full QTF match very well between NEMOH and Orcawave. Slight differences are visible around the resonant peak but at other frequencies match quite well.

This comparison between NEMOH and Orcawave supports the validity of both software. In the following works, Orcawave is used for a couple of reasons. The first is that Orcawave has the capability to generate its own free-surface mesh, while a discretized free surface mesh from an external mesher is required to be imported into NEMOH. Additionally, the 2^{nd} part of the thesis is made easier due to Orcawave's synergy with Orcaflex, which is used for time-domain simulations.

4 QTF ANALYSIS OF A HEAVY LIFT VESSEL

This chapter has been redacted due to the confidential nature of the thesis.

4.1 Vessel and Load Condition Definition

This section has been redacted due to the confidential nature of the thesis.

4.2 Mesh Study

This section has been redacted due to the confidential nature of the thesis.

4.2.1 Lid Mesh Study

This subsection has been redacted due to the confidential nature of the thesis.

4.2.2 Body Mesh Study

This subsection has been redacted due to the confidential nature of the thesis.

4.2.3 Free Surface Mesh Study

This subsection has been redacted due to the confidential nature of the thesis.

4.3 Diffraction Analysis

This section has been redacted due to the confidential nature of the thesis.

4.3.1 Roll RAOs (1^{st} Order Results)

This subsection has been redacted due to the confidential nature of the thesis.

4.3.2 Roll QTFs (2^{nd} Order Results)

This subsection has been redacted due to the confidential nature of the thesis.

4.4 Comparison of 1st and 2nd Order Loads

This section has been redacted due to the confidential nature of the thesis.

4.5 Estimation of Significant Roll Responses

This section has been redacted due to the confidential nature of the thesis.

5 TIME-DOMAIN SIMULATIONS AND OPERABILITY STUDY

This chapter has been redacted due to the confidential nature of the thesis.

5.1 Simulation Setup

This section has been redacted due to the confidential nature of the thesis.

5.2 Roll Motion Time-History

This section has been redacted due to the confidential nature of the thesis.

5.3 Roll Motion Spectrum

This section has been redacted due to the confidential nature of the thesis.

5.4 Operability Study

This section has been redacted due to the confidential nature of the thesis.

5.4.1 Most Probable Maximum Roll Motion

This subsection has been redacted due to the confidential nature of the thesis.

5.4.2 Limiting Significant Wave Heights

This subsection has been redacted due to the confidential nature of the thesis.

6 CONCLUSIONS & FUTURE WORK

This chapter has been redacted due to the confidential nature of the thesis.

ACKNOWLEDGMENTS

I would like to express my profound gratitude to my mentor at DEME Offshore, Alufa Samson Olorunfemi, for your consistent support, advice, and guidance throughout this master thesis. Your patience and constant support have been essential in navigating through this challenging topic and completing the thesis. A special note of thanks to Benjamin Baert who has given me the opportunity to pursue this master thesis research under his excellent naval team at DEME Offshore. I would also like to acknowledge and appreciate my naval team colleagues Florian, David, Elstine, Christophe, Per, Rita, Andrea, Stijn, Jens, and Massami for their availability and willingness to answer my questions, making my thesis internship a pleasant experience.

I would like to extend my deepest gratitude to Professor Philippe Rigo, initiator and coordinator of the EMShip+ program, for graciously allowing me the opportunity to enroll in the program despite my previously misaligned professional background. His belief in me has opened new doors for which I will be forever grateful. I would also like to thank Prof. Lionel Gentaz for his continuous support and for allowing me the privilege to attend the eye-opening lectures at ECN. I am equally thankful to the professors at ULiege and ECN for their excellent teaching and guidance.

I would like to appreciate my EMShip+ cohort, the last cohort under the coordination of Prof. Rigo. The time we spent shared together studying, working, and hanging out will always be cherished and unforgettable years.

Finally, my heartfelt appreciation goes to my wife, whose love and support have been my driving force throughout this master program. Your encouragement and belief has provided the motivation to complete this work.

Bibliography

[1] Yongui Liu. "On Second-Order Roll Motions of Ships". In: June 2003.

[2] Flavia Rezende, Xiaobo Chen, and Marcos D Ferreira. "Simulation of Second-Order Roll Motions of a FPSO". In: June 2008. DOI: 10.1115/OMAE2008-57405. URL: https://doi.org/10.1115/OMAE2008-57405.

[3] Johannes Albert Pinkster. "Low Frequency Second Order Wave Exciting Forces on Floating Structures". PhD thesis. Netherlands: Technische Universiteit Delft, 1980. 211 pp.

[4] Bernard Molin. *Offshore Structure Hydrodynamics*. Cambridge University Press, 2023.

[5] Odd Magnus Faltinsen. *Sea Loads on Ships and Offshore Structures*. Cambridge University Press, 1990.

[6] Vincent Leroy. "Wave-structure interaction". Fall semester wave-structure interaction course notes at ECN, 2024.

[7] TU Delft. "Chapter 9: Non-Linear Behaviour and Chapter 10: Operability". Extract of TU Delft's Open Course Ware on Offshore Hydromechanics. URL: https://ocw.tudelft.nl/wp-content/uploads/Part_3.pdf.

[8] Ansys Inc. *AQWA Theory Manual*. 2023.

[9] Ruddy Kurnia and Guillaume Ducrozet. *NEMOH v3.0 User Manual*. Tech. rep. École Centrale de Nantes, 2022. DOI: 10.13140/RG.2.2.12752.28162.

[10] Orcina Ltd. *Orcawave web help*. 2025. URL: https://www.orcina.com/webhelp/OrcaWave/.

[11] Orcina Ltd. *Orcaflex web help*. 2025. URL: https://www.orcina.com/webhelp/OrcaFlex/.

[12] DNVGL. *DNVGL-RP-C205: Recommended Practice Environmental Conditions and Environmental Loads*. 2017.

[13] Allan C. Oliveira, Luiz Felipe P. Carvalho, and Fabio G. T. Menezes. "Standardizing Second-Order Roll Analyses for FPSOs in Brazilian Deep and Ultra Deep Waters: Approximations and Damping Evaluation". In: June 2024.

[14] Ruddy Kurnia, Guillaume Ducrozet, and Jean-Christophe Gilloteaux. *Second Order Difference- and Sum-Frequency Wave Loads in the Open-Source Potential Flow Solver NEMOH*. Hamburg, Germany, June 2022. DOI: 10.1115/OMAE2022-79163.hal-03846967. URL: https://hal.science/hal-03846967/document.

[15] Ruddy Kurnia and Guillaume Ducrozet. "NEMOH: Open-source boundary element solver for computation of first- and second- order hydrodynamic loads in the frequency domain". In: *Computer Physics Communications* (2023). URL: https://www.sciencedirect.com/science/article/pii/S0010465523002308.

[16] Flavia Rezende, Allan Oliveira, Xiaobo Chen, and Fabio Menezes. "A Comparison of Different Approximations for Computation of Second Order Roll Motions for a FLNG". In: June 2013. DOI: 10.1115/OMAE2013-11004. URL: https://doi.org/10.1115/OMAE2013-11004.

[17] Guillaume Hautecloque, Olaf Waals, Flavia Rezende, and Xiaobo Chen. "Review of Approximations to Evaluate Second-Order Low Frequency Load". In: July 2012. DOI: 10.1115/OMAE2012-83407. URL: https://doi.org/10.1115/OMAE2012-83407.

[18] Line Roald, Jason Jonkman, Amy Roberston, and Ndaona Chokani. "The effect of second-order hydrodynamics on floating offshore wind turbines". In: vol. 35. Jan. 2013, pp. 253–264. DOI: 10.1016/j.egypro.2013.07.178. URL: https://doi.org/10.1016/j.egypro.2013.07.178.

[19] Bayati et al. "The effects of second-order hydrodynamics on a semisubmersible floating offshore wind turbine". In: *Journal of Physics: Conference Series* (2014). DOI: 10.1088/1742-6596/524/1/012094.

[20] Espen Engebretsen, Zhiyuan Pan, and Nuno Fonseca. "Second-Order Difference-Frequency Loads on FPSOs by Full QTF and Relevant Approximations". In: Aug. 2020. DOI: 10.1115/OMAE2020-18132. URL: https://doi.org/10.1115/OMAE2020-18132.

[21] LHEEA. *NEMOH*. URL: https://gitlab.com/lheea/Nemoh. (accessed: February 3, 2025).

[22] LHEEA. *meshmagick*. URL: https://lheea.github.io/meshmagick/. (accessed: February 9, 2025).